

Synthesis of Activated Carbon/Chitosan Composites and Expanded Graphite for Symmetric Supercapacitor

Galen Noel G Nifas* and Rex S Forteza

Philippine Science High School-Central Luzon Campus, Mabalacat City, Pampanga, 2010 Philippines, Philippines

Abstract

Supercapacitors have great electrochemical characteristics such as high energy and power densities, charge-discharge rates, and extremely long cycle life which make them favourable in electronics and other applications. Activated carbon was successfully coated with chitosan, and natural graphite flakes were chemically and thermally modified into expanded graphite; these were structurally and morphologically analysed using FTIR and SEM. FTIR analysis showed the presence of N-H scissoring from amine and amide groups, C-O and C≡C stretching for activated carbon/chitosan (AC/CH) composites and OH group, C=C and C-O stretching for expanded graphite (EG). SEM images show that AC/CH and EG have porous structures; AC/CH has chitosan chunks on activated carbon surface. The fabricated supercapacitors were tested for their specific capacitances, charging rates, and energy and power densities. At potential window of 0.001 V, the lowest specific capacitance, charging rate, energy density, and power density are 0.49 ± 0.0060 F/g, 0.12 ± 0.0018 mC/s, 6.853×10^{-8} Wh/kg, and 1.556×10^{-4} W/kg, respectively, which are obtained from 100% EG treatment. The symmetric supercapacitors can reach a specific capacitance of 272 ± 14.47 F/g, charging rate of 65.3 ± 0.81 mC/s, and energy density of 3.786×10^{-5} Wh/kg and power density of 0.0817 W/kg with 50% AC/CH-50% EG treatment.

Keywords: Supercapacitor; Activated carbon/chitosan composites; Expanded graphite; Specific capacitance; Charging rates; Energy density; Power density

Introduction

The development of portable and wearable energy electronic devices showed great convenience in real life application but demanded large amount of energy. In response, developing and refining highly efficient energy storage devices become an important issue [1]. Such energy storage devices are extensively developed towards light-weight, flexible, and high power density devices [2]. Supercapacitors utilize high surface area electrode materials and thin electrolytic dielectrics to harvest higher magnitudes of capacitance than that of conventional capacitors. Also, supercapacitors exhibit greater power density, higher energy density, longer cycle life, and excellent pulse charge-discharge property compared to conventional capacitors. Compared to traditional supercapacitors, solid-state supercapacitors use gel polymer electrolyte which makes the supercapacitor flexible, wearable, and environmental friendly [3]. In traditional capacitors, electrons transfer from one electrode to another separated by solid dielectric; the use of ion rich-liquid electrolytes that act as an extremely thin dielectric for supercapacitors results to the higher capacitance of the latter device. Unlike batteries, the charge-discharge process of super capacitors involves no chemical reactions, thereby, resulting to minimal to no chemical degradation of compounds inside the device. Supercapacitors can potentially be utilized in back-up power storage, lightweight electronic fuses, peak power sources, and hybrid power sources.

Activated carbon possesses higher surface area and is more cost efficient as compared with other carbon-based material which makes them commonly used as an electrode material for supercapacitors. Generally, higher surface area equates higher capacitance; however, not all of the high surface area of the activated carbon contributes to the capacitance of the device since some pores are prevented to participate in charge storage because of electrolyte ions that are too large to diffuse into smaller micropores. Due to this, impregnation of substances, to the pores of the carbon are used to improve the existing properties of the activated carbon by providing synergism between the chemical

and the carbon [4]. Impregnation of chitosan on activated carbon produced an activated carbon/chitosan composite with higher surface area than activated carbon alone; from $301.9 \text{ m}^2/\text{g}$ of naked activated carbon, the coated activated carbon had a surface area of $531.3 \text{ m}^2/\text{g}$ [5]. Since chitosan is the second most abundant polysaccharide; it is of high interest in the field of research due to its high natural abundance, biocompatibility, biodegradability, and non-toxicity [6].

Graphite-based materials have become an essential material for supercapacitor electrode due to its exceptionally high power performance, high mechanical strength, excellent surface area, and good conductivity. The integration of graphite-based electrodes has emerged as a promising energy storage device, which hopefully can take full advantage of exclusive physical and chemical properties such as high conductivity for charge storage and large specific area [7].

Energy storage devices such as supercapacitors store energy for later use to supply utility grid or local grids. However, energy storage devices should be enhanced to exhibit excellent electrochemical properties and to utilize cost-efficient materials since such devices, nowadays, are either low in power density or high in price. The study aims to design and synthesize a solid-state supercapacitor of high specific capacitance with flexible electrode and gel polymer electrolyte which could possibly alleviate problems encountered in energy storage.

This study is designed to assemble symmetric solid-state supercapacitors using the activated carbon/chitosan composites and

*Corresponding author: Galen Noel G. Nifas, Philippine Science High School-Central Luzon Campus, Mabalacat City, Pampanga, 2010, Philippines, Tel: (+639) 165948091; E-mail: galennifas@gmail.com

Received July 24, 2019; Accepted August 22, 2019; Published August 28, 2019

Citation: Nifas GNG, Forteza RS (2019) Synthesis of Activated Carbon/Chitosan Composites and Expanded Graphite for Symmetric Supercapacitor. J Material Sci Eng 8: 534.

Copyright: © 2019 Nifas GNG, et al. This is an open-access article distributed under the terms of the Creative Commons Attribution License, which permits unrestricted use, distribution, and reproduction in any medium, provided the original author and source are credited.

expanded graphite with varying ratios as active components for the supercapacitor electrodes and to compare their specific capacitances. This research aims to measure the capacitance, charge rate, energy density, and power density of the fabricated supercapacitors using linear voltammetry and to evaluate the active components characteristics – surface morphology and structure – and relate them to the performance of the supercapacitors.

Materials and Methods

Acquisition of materials

Commercial chitosan (CH) with $\geq 75\%$ degree of deacetylation was bought from Sigma-Aldrich while aluminium foil was bought from a local store. Commercial activated carbon (AC) and natural graphite (NG) were procured from local distributors. Poly (vinyl alcohol) (PVA), H_2SO_4 , and other necessary reagents were provided by PSHS-CLC Laboratory.

Preparation of activated carbon/chitosan composite (AC/CH)

Following the protocol of Vinitnantharat et al. [8] with some modifications, chitosan gel solution was prepared by dissolving one gram of CH in 100 mL of 1% (v/v) acetic acid which was then stirred for 8 hours. AC was rinsed in distilled water and dried at $100^\circ C$ in an oven for 6 hours. The washed AC was mixed with 1% (w/v) NaOH solution for 8 hours which was filtered through filter paper and dried up afterwards. The dried AC was placed into the chitosan gel solution in the ratio 2(AC):1(CH) and agitated for 8 hours. The obtained mixture was neutralized by rinsing for several times using distilled water followed by air drying.

Synthesis of expanded graphite (EG)

Expanded Graphite (EG) was prepared via exfoliation of NG flakes according to the study of Yue et al. [9]. 6.0 g of NG flakes was added to 10 mL of concentrated H_2SO_4 as the intercalating agent and 1.5 mL of 30% v/v H_2O_2 as the oxidizing agent. The mixture was mixed for 90 minutes at $50^\circ C$ which was then washed using distilled water until pH 5-7. The washed mixture was filtered and oven-dried at $70^\circ C$ for 24 hours and was abruptly heated at $400^\circ C$ for 45 seconds afterwards.

Preparation of electrode materials

Four ratios of AC/CH to EG were prepared as electrode materials with a total of 0.4 g of active materials – 0.2 g for each side of the supercapacitor. Two sets of 0.2 g of EG, 0.16 g of EG and 0.04 g AC/CH, 0.10 g EG and 0.10 g AC/CH, and 0.04 g EG and 0.16 g AC/CH were measured to prepare 100, 80, 50 and 20% by mass of EG to the total mass of active materials.

Fabrication of AC/CH and EG-based symmetric supercapacitor

Two pieces of 1 inch by 1 inch aluminium foil were used as current collectors in a symmetric cell configuration. The electrolyte was prepared by mixing 5 g PVA, 5 g H_2SO_4 , and 50 mL distilled water; the mixture was stirred vigorously at $85^\circ C$ until it becomes transparent. The electrolyte was casted on the symmetric electrodes after putting the electrode materials on the current collector. The two halves of the device were assembled together after the evaporation of solvent in the electrolyte; three pieces of lens tissue paper were inserted between the two electrodes as the separator in the supercapacitor as depicted in Figure 1. 100% EG, 80% EG-20% AC/CH, 50% EG-50% AC/CH, and 20% EG-80% AC/CH supercapacitors were named as Negative Control, Treatment 1, 2, and 3, respectively.

Data collection

FTIR analysis: Small amounts of the composite were analysed. Results of FTIR analysis came in the form of images and were analysed by the researcher.

SEM imaging: Small amounts of the composite were analysed. The results of SEM were sent via email in the form of images.

Specific capacitance and charging rates tests: The supercapacitors were tested using Bio-logic Galvanostat/Potentiostat with three-point connection configuration. At 0.001 V and 1 mV/min, the $Q-Q_0$ vs. time plot was generated by the apparatus. The results were obtained in Tabular Form for the obtained values such as the $Q-Q_0$, slope and correlation (r^2 value) of lines and in the form of images for the $Q-Q_0$ vs. time plot.

Data analysis

FTIR analysis: The results of FTIR analysis for the expanded graphite were compared to published FTIR spectra for expanded graphite while the FTIR spectrum of activated carbon/chitosan composite was compared to the FTIR spectra of standard activated carbon and chitosan and to an FTIR spectrum from a published journal. The resulting FTIR peaks of the expanded graphite and the composites were tabulated and were compared among each other. The presence of certain functional groups represent the structural components found in the sample and may prove the physical or chemical reaction between or among the compounds.

SEM imaging: SEM imaging was analysed according to the surface morphology seen in the image. The change in the apparent texture, the pore structure, and the interaction of compounds on the surface of another compound can be seen in the SEM imaging in correspondence to the known characteristics of the compounds in the samples.

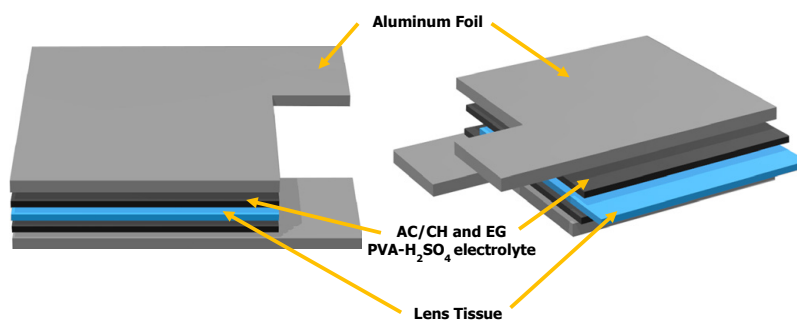


Figure 1: Diagram of the symmetric solid-state supercapacitor.

Specific capacitance and charging rates tests: The specific capacitances and the charging rates of the fabricated supercapacitors were evaluated using the equations for capacitance and by obtaining the slopes of the line in $Q-Q_0$ vs. time graphs:

$$C_s = \frac{Idt}{m\Delta V} \quad (1)$$

$$r_Q = \frac{dQ}{dt} = \left| \frac{Q - Q_0}{t_0 - t_1} \right| \quad (2)$$

Where C_s is specific capacitance and r_Q is the charging rate of the supercapacitors, $Q-Q_0$ is the maximum amount of charge the supercapacitor can hold, E_1 is the vertex potential, E_2 is the initial potential, m is the mass of the active materials, t_0 is starting time of charging, and t_1 is the time when the supercapacitor reaches its maximum amount of charge.

Energy and power density: The energy capacities of the supercapacitors were characterized by the energy density of the device while the discharge rates were indicated by the power density. The following equations were used to calculate the energy and power density of the fabricated supercapacitors:

$$E = \frac{1}{2} CV^2 \quad (3)$$

$$P = \frac{E}{t} \quad (4)$$

Such that E and P are the energy and power density respectively, C is the capacitance of electrode, V is the working voltage, and t means the charging/discharging time.

Demo application: The fabricated supercapacitors were charged using a power generator at a potential window of 2.2 V for 1 minute. The supercapacitors were discharged by lighting an LED lights; the time of full discharge was not measured.

Statistical analysis: Each fabricated supercapacitor has three technical replicates. The specific capacitance and charging rate for each fabricated supercapacitor with varying ratios of activated carbon/chitosan composites and expanded graphite were measured and statistically compared using One-Way Analysis of Variance (ANOVA) with $\alpha = 0.05$ to determine if there is, at least one, significant difference among the obtained results. Moreover, Tukey's Honest Significant

Difference (HSD) tests were used to determine in which specific capacitance/s of supercapacitors a significant difference occur.

Results and Discussion

Results of the study

Structural characterization of active materials: The FTIR spectrum of the synthesized activated carbon/chitosan composites in comparison with the FTIR spectra of the commercial activated carbon and commercial chitosan was shown in Figure 2a while the comparison of the FTIR spectra of commercial natural graphite flakes with the expanded graphite in Figure 2b.

Morphological characterization of active materials: The SEM micrographs of the AC/CH at 2500x and 5000x magnification were shown in Figure 3a. Figure 3a showed the presence of the pores in the surface of AC/CH composite. The cross section of micrographs of the composite showed the presence of fine particles on the surface of the activated carbon.

The SEM micrographs of EG at 1000x, 2000x, 5000x, and 10000x magnification were displayed in Figure 3b. The SEM micrographs of EG show that EG possesses rough surface with several pores of different sizes and stacked layers of particles of different sizes.

Electrochemical tests for supercapacitors and statistical analysis: The amount of charges in the fabricated supercapacitors vs. charging time are plotted in Figures 4a-4d. The negative control, treatments 1, 2, and 3 have specific capacitances of 493.4 ± 6.00 mF/g, 13.4 ± 0.31 F/g, 272 ± 14.47 F/g, and 55.0 ± 7.36 F/g, respectively. At increasing amounts of AC/CH in the supercapacitors, the charging rates are obtained to be 0.12 ± 0.0018 mC/s, 3.4 ± 0.78 mC/s, 65.3 ± 0.81 mC/s, and 13.5 ± 1.87 mC/s, respectively; these values are the slopes of the lines in Figures 4a-4d.

The summary of data on specific capacitances, charging rates, energy densities and power densities of supercapacitors is presented in Table 1. Treatment 2 has the highest specific capacitance and charging rate while the negative control has the lowest. Based from the results of One-Way ANOVA and Tukey HSD tests, the fabricated supercapacitors can store significantly different maximum amounts of charges except when the negative control and treatment 1 are compared since the two supercapacitors have no significant difference in their

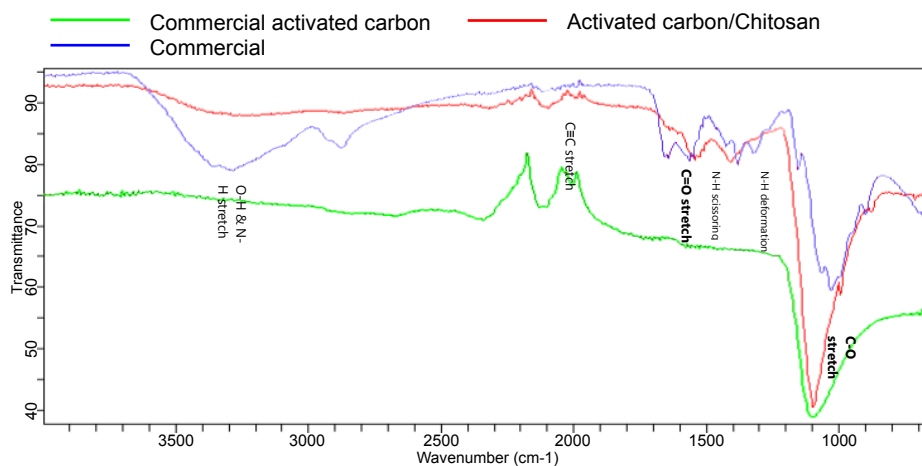
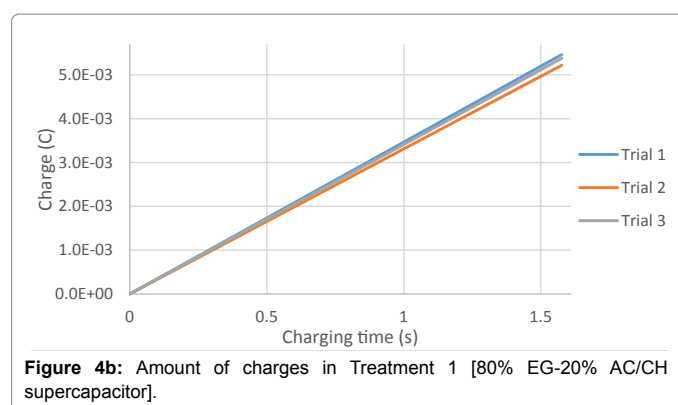
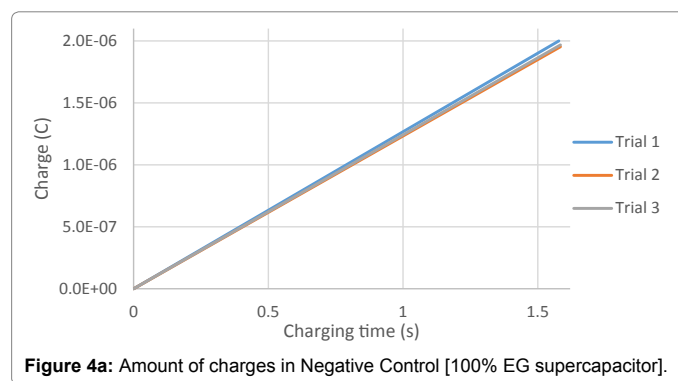
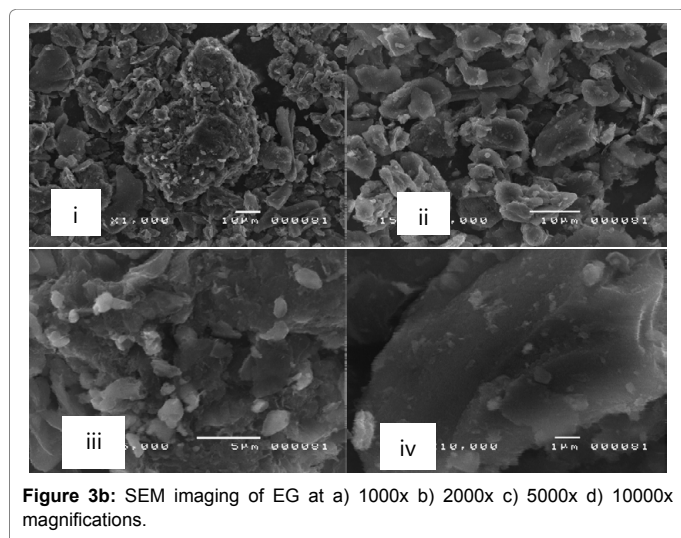
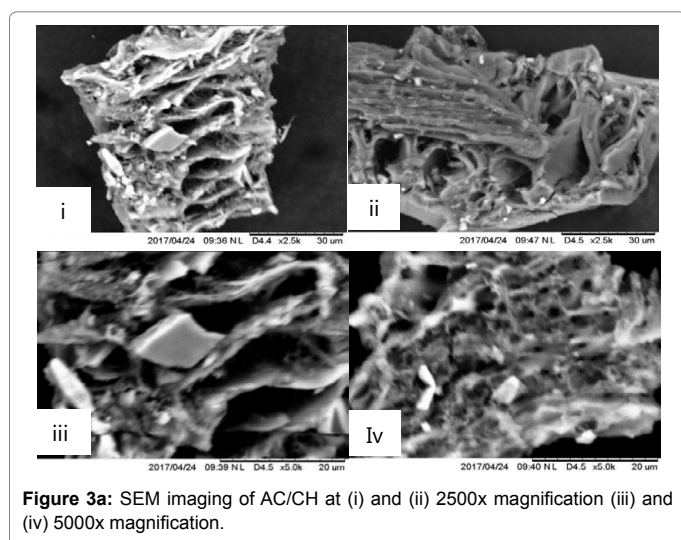
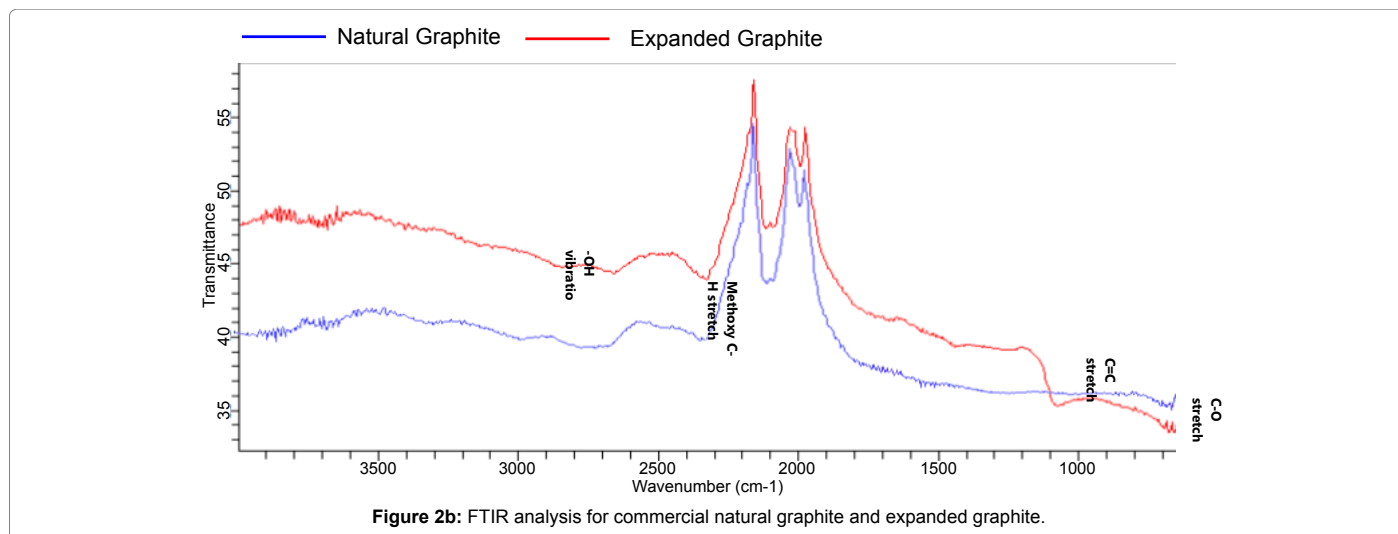


Figure 2a: FTIR analysis for commercial activated carbon, commercial chitosan, and activated carbon/chitosan composite.



time since all of their charging rates are significantly different. With these values, Treatment 2 possesses the highest energy density of 3.786×10^{-5} Wh/kg and power density of 0.0817 W/kg. Treatment 3 has the next highest energy (7.635×10^{-6} Wh/kg) and power (0.0169 W/kg) densities, which is followed by Treatment 1 (with an energy density of 1.858×10^{-6} Wh/kg and power density of 0.0042 W/kg). The negative control has the lowest energy (6.853×10^{-8} Wh/kg) and power (1.556×10^{-4} W/kg) densities among the fabricated supercapacitors.

Discussion of the results

Structural characterization of active materials: The FTIR spectrum for commercial CH displays absorption band at approximately

specific capacitances. On the other hand, the supercapacitors can reach their maximum storage capacity of charges in different durations of

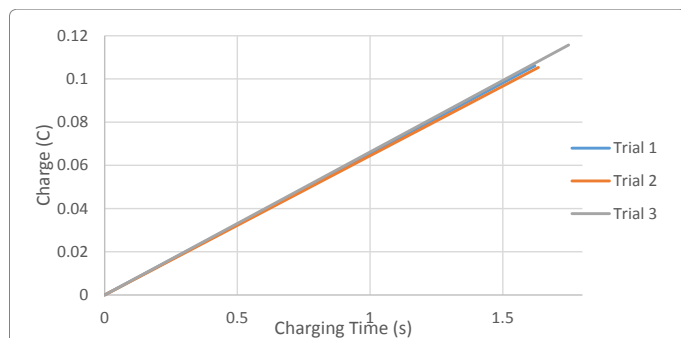


Figure 4c: Amount of charges in Treatment 2 [50% EG-50% AC/CH supercapacitor].

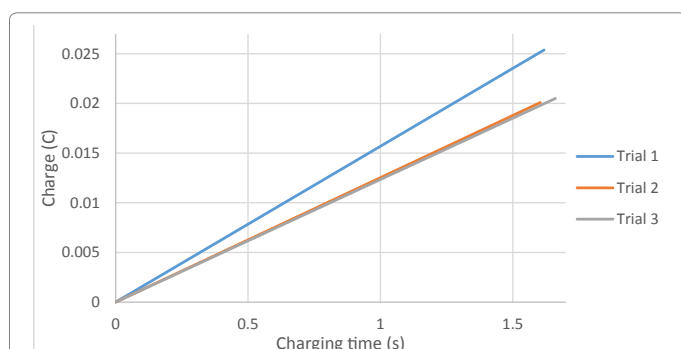


Figure 4d: Amount of charges in Treatment 3 [20% EG-80% AC/CH supercapacitor].

	Specific Capacitance (F/g)	Charging Rate (mC/s)
Negative Control	0.49 ± 0.006 ^c	0.12 ± 0.0018 ^d
Treatment 1	13.4 ± 0.31 ^c	3.4 ± 0.078 ^c
Treatment 2	272 ± 14.47 ^a	65.3 ± 0.81 ^a
Treatment 3	55.0 ± 7.36 ^b	13.5 ± 1.87 ^b

Means with the same letter (superscript) are not significantly different.

Table 1: Summary and results of One-Way ANOVA and Tukey HSD Test of specific capacitances and charging rates and of the fabricated supercapacitors.

3431 cm^{-1} due to the overlap of O-H and N-H stretching vibrations of certain functional groups engaged in H-bond. There is a peak in 1641-1653 cm^{-1} signifying the presence of C=O specifically found in amide group of CH; this band is also found in the spectra of AC and AC/CH composites. Absorption band at 1391 cm^{-1} confirms the N-H deformation vibration in $-\text{NH}_2$ while the bends at 1068-1035 cm^{-1} present the existence of skeletal vibration involving C–O stretching which is common in chitosan saccharide structures; these peaks are exhibited by AC/CH and CH. The vibrations in the range 1548-1602 cm^{-1} of the AC/CH and CH spectra represent bands indicating the presence of N-H scissoring from amine and amide groups. On the other hand, AC and AC/CH exhibit a similar peak at 2100-2260 cm^{-1} , indicating the presence of C=C stretching. The weak bands at 1641-1653 cm^{-1} in the FTIR spectrum of all powdered materials – AC, CH, and AC/CH – represent the stretching vibrations of C=O specifically in carbonyl, lactone, and carboxyl groups, and the C–O stretching or O-H deformation in carboxylic acids, respectively.

The FTIR spectrum of the CH is nearly identical to that in Soni et al. [10] and Shariffard et al. [11]. This confirms that the used chitosan is appropriate for the preparation of one of the supercapacitor active materials, the activated carbon/chitosan composites. However, the AC

and AC/CH composites are relatively different but are similar to certain peaks compared to Soni et al. [10] and Shariffard et al. [11]. This is accounted from the different qualities of reagents for the activation process (physical or chemical) for the commercial activated carbon and the minor modifications in the synthesis of activated carbon/chitosan composites. Some aliphatic and aromatic functional groups are absent in the activated carbon since the chemical activation breaks several bonds in aliphatic and aromatic substances; chemical activation also eliminates volatile and light substrates. The FTIR spectrum of AC/CH is a hybrid of the spectra of commercial chitosan and commercial activated carbon – some peaks of the composite are present on the aforementioned materials individually. The C–O stretching and N-H scissoring from amine and amide groups of AC/CH are from CH while the present C=C stretching in AC/CH comes from AC. Moreover, the presence of N-H scissoring from amine and amide groups validates the activated carbon indeed is coated with chitosan. Patkool, et al. [5] concluded that impregnation of chitosan on activated carbon will have more amino ketone and aldehyde group when compared to the original activated carbon substrate.

There are present peaks at 3405 cm^{-1} and 1634 cm^{-1} for natural graphite flakes and expanded graphite indicating –OH vibration and C=C stretching, respectively. The following changes were observed in the FTIR spectra of EG after the exfoliation of NG: a new absorption band emerged at 1035-1068 cm^{-1} representing CO stretching. Also, the methoxy C–H stretch at 2850-2950 cm^{-1} can be observed in the FTIR spectrum of NG and EG; the peak at this wavenumber is gentler at the spectrum of EG.

The presence of –OH group, C–H stretching, and C=C stretching on NG and EG confirms the identities of the two graphite materials [12]. The existence of C–O stretching on EG is caused by the oxidation of NG by H_2O_2 and high temperature expansion. The FTIR spectrum of NG has sharper peak for the alkyl C–H stretching since EG underwent oxidation and abrupt expansion under high temperature which can break some of the C–H functional groups in EG. Nonetheless, the FTIR spectra of NG and EG are similar in majority of their peaks.

Morphological characterization of active materials: The particles shown in Figure 3a(i) can be inferred as a fraction of chitosan that penetrated into the inner sites of the activated carbon. The chitosan chunks on the surface of the activated carbon rods are different in sizes. As seen in Figure 3a(i-iv), there are different sizes of pores in the activated carbon which further explains why there are different sizes of chitosan particles present on the carbon's surface.

In Figure 3b(ii) and 3b(iii), several layers of stacked particles of EG are present due to the exfoliation of NG when NG was oxidized and expanded under high temperature. The high porosity and rough surface characteristic of EG accounts from the several chemical processes undergone to prepare EG. There are different sizes of stacked particles of EG since not all parts of graphite are equally exposed to the intercalating and oxidizing agents during stirring and to heat in the furnace during the abrupt heating.

Electrochemical characterization of supercapacitors: Since the active materials of the fabricated supercapacitors – AC/CH and EG – are highly porous, there is a high amount of charges that can be accommodated to their surfaces leading to higher capacitance of the supercapacitor. The difference in ratios of two active materials – while maintaining the combined mass of the active materials constant – resulted to a significant difference in the obtained capacitances. Since activated carbon/chitosan composites can possess a higher pore

volume ($0.29 \text{ cm}^3/\text{g}$) and surface area ($531.3 \text{ m}^2/\text{g}$) [5] compared to the pore volume ($0.008 \text{ cm}^3/\text{g}$) and surface area ($21.564 \text{ m}^2/\text{g}$) of expanded graphite [13], increasing the amount of AC/CH will result to a higher pore volume and surface area for the electrode of the supercapacitor. The pore volume and surface area of the active materials have a positive relationship with the capacitance of the supercapacitor [14]; this explains the increasing capacitances for the negative control, Treatments 1 and 2. However, there is an observed decrease in specific capacitance on Treatment 3. Even though there is a higher amount of AC/CH in Treatment 3 than in Treatment 2, the significant drop in the capacitance can be explained by the presence of low amounts of EG which act as the conductive material for the pathway of charges. The electrical conductivity of chitosan at room temperature ranges from 10^{-10} to 10^{-9} S/cm [15] while the electrical conductivity of activated carbon is 0.40 S/cm [16]; both activated carbon and chitosan have low electrical conductivity which makes it difficult for charges to diffuse to the available surface in the active materials of Treatment 3. As compared to the fabricated supercapacitors with higher amounts of EG than AC/CH, the high electrical conductivity of EG [17] gave the aggregate of active materials its relatively high electrical conductivity, thus, charges can occupy more available surface of the active materials of the supercapacitors.

At a constant scan rate of $1 \text{ mV}/\text{min}$ and potential window of 0.001 V , the significant rise of charging rates in the negative control, treatments 1 and 2 is due to the slowing down of positive and negative charges when separating during charging of the supercapacitors—positive charges going on one side and negative charges on the other. The available sites in the surface of the active materials in each electrode are being accommodated by charges; for a supercapacitor with active materials of lower porosity and surface area, it will be more difficult for the charges to arrange themselves when the voltage is applied during charging which leads to slower charging rates. The statistically substantial drop in the charging rate of Treatment 3 is accounted from the same explanation on the decrease of its capacitance; the lower electrical conductivity of its active materials compared to that of Treatment 2 explains why charging the former is slower than charging the latter supercapacitor. On the other hand, the high surface area of the active materials in Treatment 3 and the high electrical conductivity of EG give this supercapacitor a higher charging rate than the negative control and treatment 1.

The energy and power density of the fabricated supercapacitors are lower than the supercapacitors from other literatures – activated carbon/graphene hydrogel supercapacitor with highest power density of $3140 \text{ W}/\text{kg}$ and energy density $9.8 \text{ Wh}/\text{kg}$ [18] and graphene oxide-chitosan hydrogel supercapacitor with highest power density of $13.95 \text{ Wh}/\text{kg}$ and energy density of $0.7 \text{ kW}/\text{kg}$ [7] because of the low potential window used during the testing in this research. The low energy and power densities do not necessarily mean that the supercapacitors have poor energy-power combination due to ion diffusion resistances, torturous afflicting diffusion pathways within porous textures, or other poor interactions. The high specific capacitance values of the supercapacitors can show that there is a good interaction of the active materials that is suitable for holding high amount of charges.

Conclusion

The active electrode materials were successfully prepared; chitosan was coated to activated carbon and natural graphite flakes were exfoliated and expanded to form expanded graphite based from the results of FTIR analysis and SEM imaging. Furthermore, supercapacitors were

fabricated using varying ratios of AC/CH and EG and PVA- H_2SO_4 gel polymer as the electrolyte. 50% EG-50% AC/CH supercapacitor has the highest specific capacitance and charging rate of $272 \pm 14.47 \text{ F}/\text{g}$ and $65.3 \pm 0.81 \text{ mC}/\text{s}$. The other fabricated supercapacitors have specific capacitance and charging rates of $55.0 \pm 7.36 \text{ F}/\text{g}$ and $13.5 \pm 1.87 \text{ mC}/\text{s}$ for 20% EG-80% AC/CH supercapacitor, $13.4 \pm 0.31 \text{ F}/\text{g}$ and $3.4 \pm 0.078 \text{ mC}/\text{s}$ for 80% EG-20% AC/CH supercapacitor, and $0.49 \pm 0.0060 \text{ F}/\text{g}$ and $0.12 \pm 0.0018 \text{ mC}/\text{s}$ for 100% EG supercapacitor. Moreover, 50% EG-50% AC/CH supercapacitor has the highest energy density of $3.786 \times 10^{-5} \text{ Wh}/\text{kg}$ and power density of $0.0817 \text{ W}/\text{kg}$ among the supercapacitors. The relatively low energy and power densities of the fabricated supercapacitors is a result of the low potential window (0.001 V) used during the electrochemical testing.

Acknowledgments

We show appreciation to the SRAs of our laboratory for their guidance while we were in the laboratory. To PSHS-CLC and DLSU, we are thankful for letting us use your facilities. Lastly, we want to acknowledge my family and friends for staying with us during the entirety of our study.

References

1. Beka L, Liu W, Xin L (2017) Nickel cobalt sulfide core/shell structure on 3D graphene for supercapacitor application. *Scientific Reports*.
2. Liu, Chang (2015) Polyaniline and Graphene Based Symmetric and Asymmetric Solide-State Supercapacitors. (Electronic Thesis or Dissertation).
3. Yu C, Ma P, Zhou X, Wang A, Qian T, et al. (2014) All-solid-state flexible supercapacitors based on highly dispersed polypyrrole nanowire and reduced graphene oxide composites. *ACS Appl Mater Interfaces* 6: 17937-43.
4. Henning K, Schafer S (1993) Impregnated activated carbon for environmental protection. *Gas Separation & Purification* 7: 235-240.
5. Patkool C, Chawakitchareon P, Anuwattana R (2014) Enhancement of efficiency of activated carbon impregnated chitosan for carbon dioxide adsorption. *Environ Eng Res* 19: 289-292.
6. Zhang HL, Wu SH, Tao Y, Zang LQ, Su ZQ (2009) Preparation and characterization of water-soluble nanoparticles as protein delivery system. *Journal of Nanomaterials* 2010: 5.
7. Sun G, Li B, Ran J, Shen X, Tong H (2015) Three-dimensional hierarchical porous carbon/graphene composites derived from graphene oxide-chitosan hydrogels for high performance supercapacitors. *Electrochimica Acta* 171: 13-22.
8. Vinitnantharat S, Rattanasirisophon W, Ishibashi Y (2007) Modification of granular activated carbon surface by chitosan coating for geosmin removal: sorption performances. *Water Sci Technol* 55: 145-152.
9. Yue X, Duan W, Lu Y, Zhang F, Zhang R (2011) Effect of ZnO loading technique on textural characteristic and methyl blue removal capacity of exfoliated graphite/ZnO composites. *Bulletin of Materials Science* 34: 1569-1573.
10. Soni U, Bajpai J, Bajpai A (2015) Chitosan-Activated Carbon Nanocomposites as Potential Biosorbent for Removal of Nitrophenol from Aqueous Solutions. *Int J Nanomaterials Biostructures* 53-61.
11. Shariffard H, Ashtiani F, Soleimani M (2012) Adsorption of palladium and platinum from aqueous solutions by chitosan and activated carbon coated with chitosan. *Asia-Pacific J Chem Eng* 8: 384-395.
12. Mohan S, Bhanuprakash L, Subash C, Varghese S (2014) Short beam Shear strength measurements of Glass fibre reinforced Epoxy Nanocomposites modified with Graphene Oxide interfaces. *Int J Chem Tech Research* 6: 1693-1695.
13. Zhang Z, Fang X (2006) Study on paraffin/expanded graphite composite phase change thermal energy storage material. *Energy Conversion & Management* 47:303-310.
14. Raymundo PE, Kierzek K, Machnikowski J, Beguin F (2006) Relationship between the nanoporous texture of activated carbons and their capacitance properties in different electrolytes. *Carbon* 44: 2498-2507.
15. Aziz N, Majid S, Yahya R, Arof A (2009) Conductivity, structure, and thermal

- properties of chitosan-based polymer electrolytes with nanofillers. *Polymer Advanced Technologies* 22: 1345-1348.
16. Zhang X, Wang Q, Xia X, He W, Huang X, et al. (2017) Addition of conductive particles to improve the performance of activated carbon air-cathodes in microbial fuel cells. *Environmental Research Water Research & Technology* 3: 806-810.
17. Dhakate S, Sharma S, Borah M, Mathur R, Dham T (2008) Expanded graphite-based electrically conductive composites as bipolar plate for PEM fuel cell. *Int J Hydrogen Energy* 33: 7146-7152.
18. Ates M, Cinar D, Caliskan S, Gecgel U, Uner O, et al. (2016) Active carbon/graphene hydrogel nanocomposites as a symmetric device for supercapacitors. *Fullerenes, Nanotubes, and Carbon Nanostructures* 24: 427-434.